Frontiers in Scientific Research and Technology

Online ISSN: 2682-297
Print ISSN: 2682-2962
http://fsrt.journals.ekb.eg

FSRT J 4 (2022) 62 - 81 10.21608/FSRT.2022.152965.1067

Characterization and Evaluation of Groundwater in Wadi Abu Gurdi, West Baranis area, South Eastern Desert Egypt: Geophysical and Hydrogeochemical Investigations

Ahmed K. Alezabawy, Mohamed Ammar, Alhussein Adham Basheer

Geology Department, Faculty of Science, Helwan University, 11790 Ain Helwan, Cairo, Egypt.

ARTICLE INFO

Article history:
Received 28 July 2022
Received in revised form 2 August 2022
Accepted 4 August 2022
Available online 7 August 2022

Keywords
Geophysical investigation;
Groundwater;
Ion exchange;
Arid area;
Hydrogeochemistry

ABSTRACT

Information collected from geophysical and geochemical data has been used in investigating the groundwater resources potential, hydrogeochemical characteristics, major hydrogeochemical processes that govern groundwater chemistry, quality and suitability assessment for drinking and irrigation uses from six wells of shallow quaternary aquifer in southern part of Eastern Desert, Egypt. A total of 32 Time-Domain electromagnetic soundings (TDEM) in time phase and vertical electrical soundings (VES) were measured on the same sites to detect the subsurface geological section and delineate water-bearing layers. The results of geoelectrical interpretation calibrated with gamma ray and resistivity logs of drilled wells. The findings illustrated that the subsurface section has four geoelectrical layers. The second layer represents the freshwater aquifer. Our results demonstrated that the dominant hydrogeochemical facies observed in this area is Ca + Mg-Cl + SO_4 and mixed Ca + Mg-Cl + SO_4 type. According to Base Exchange index (r1) and (r2), the water classified as Na-SO_4 type, which is associated with salinization (r1<1) and deep meteoric percolation type (r2<1). The groundwater chemistry depends on reverse ion exchange weathering of carbonate minerals as well as silicate weathering. Moreover, evaporation process controlling factors of groundwater chemistry in quaternary aquifer. Results from EC, sodium adsorption ratio (SAR), soluble sodium percentage (SSP), permeability index (PI) and magnesium hazard (MH) reveal that most of groundwater is relatively appropriate for Agricultural purposes.

1. Introduction

Egypt is one of those countries that has a shortage of water, not only due to its limited water supplies but also due to its arid climate. The research area has a freshwater shortage, with rainfall behaving as the only source of drinkable water and the primary source of groundwater recharge. Groundwater is the principal resource of fresh water in Egypt's Eastern Desert, which occupies 22% of the country's total area (Ahmed et al. 2019). Many investigations have been done in latest years to better understand the evaluation of water resources in the Eastern Desert (Gheith and Sultan, 2002; Abdel Moneim 2005; Yousef et al. 2009; Abdalla, 2012; Ahmed et al. 2019). In such circumstances, establishing a groundwater quality baseline is critical.

Because fresh groundwater is scarce, a number of desalination facilities have been built to meet the rising requirement for water, particularly for drinking and household needs. From north to south, these facilities were distributed to one facility in Hamata area, one facility in Mars Homeira area and two facilities in Marsa Alam city (Arafat et al. 2017).

* Corresponding authors at Helwan University

E-mail addresses: ahmed.ezabawy@science.helwan.edu.eg (Ahmed K. Alezabawy)

Quality of groundwater normally controlled many factors, i.e water–rock interactions, recharge from different origins, lithology, and geochemical activities along the flow direction in aquifer. Hydrochemical information derived from interactions able to be used to determine hydrochemical characteristics, mechanisms and processes, origins of major ions, pollution source, and significance for irrigation, …etc. (Alemayehu et al. 2020; Yidana et al. 2020).

The current study was performed to detect the water quality and evolution based on different parameters, delineate water-bearing aquifers, and select the good locations for the future drilling plan. The novelty of the current study is to use integrated interpretation for geophysical data represented by TDEM, VES data and hydrochemistry data. The geophysical data is used for delineation of the configuration of groundwater represented by the thickness and depth of the aquifer. The hydrochemistry data is used to determine the quality of aquifer, estimate the percentage of cations and anions in the area under investigation, and then select suitable sites for drilling new wells in the stud area.

Measuring the electrical resistivity by electromagnetic in time-phase and vertical electrical sounding techniques have been generally used to solve the groundwater prospecting impediments and hydrogeology, delineate the

potentiality of groundwater in and its geology, define the aquifer, saltwater intrusion, and detect the subsurface structures (e.g., Nowroozi et al., 1999; Sultan and Santos, 2008; Araffa, 2010; Mohamed et al, 2012; Araffa et al, 2015;; Araffa et al. 2017; Basheer et al, 2020; Mosaad and Basheer, 2020; Alezabawy et al. 2021; Babatunde et al., 2022; Chouchene et al, 2022).

Methods utilized in the current study (i.e., geophysical and geochemical techniques) may be more extensively appropriate as a kind of decision-making technique. The objectives of this research were: (1) to assess the chemistry of groundwater; and (2) to detect hydrogeochemical process that presently controlled the water chemistry in the region. The quality of groundwater for human potable and agricultural uses is also taken into account.

2. Study area characteristics

The area under investigation is a located in the southern Eastern Desert (23◦ 45′ to 24◦ 3′ N and 34◦ 42′ to 34◦57′ E) covering an area of about 505 Km^2 (Fig. 1a). The area is characterized by high and low topographic lands raised above mean sea level (Fig. 1b). The highlands consist of the uplifted relief high mountains (Red Sea Hills) that located in the west side of the coastal plain. The elevation reaches roughly 1250 meters above sea level. Many drainage patterns and wadis were characterized a rugged topography (Arafat et al. 2017).

The area under investigation is distinguished by high aridity where the temperature achieves its maximum in the summer and ranges between 45 0C and 50 0C (Ageeb etal., 2007). The annual rainfall is less than150 mm/year (Khalil, 2014), while the rate of potential evaporation varies between 2.1 mm/day in winter and 9.2 mm/day in the season of summer (Mohamaden and Ehab, 2017; Ahmed et al. 2019).

Geologically, the rocks in the area under investigation are mainly composed of Precambrian basement rocks which considers as the oldest rocks on the earth (TDA/RSSTI, 2003). The Quaternary alluvial sediments are the youngest formation and widely developed with the greatest thickness towards the Red Sea coast (20m) (Abdel Moneim,2005). They are characterized by (1) Wadi deposits as sands and gravel detrital, (2) Sabkhas as fine sands, silts, silty clay, and evaporates, and finally (3) Terraces as sand, gravels, and conglomerates with some if evaporates deposits (EGSMA, 1997).The basement rocks of Baranis-Aswan Road consist of an assortment of the oldest Pan-African rock units as well as medium-grade hornblende schist, a selection of gneisses and migmatite with medium- to low-grade metavolcanic (Ali-Bik et al.,2022) (Fig. 2).

From a hydrogeological standpoint, the Quaternary aquifer present to the east are characterized by sand, gravel and clays that form Wadi-filling (Arafat et al. 2017). Rainfall is the main recharge sources for such aquifer and, in exceptional situations, flash floods. (Zagloul et al. 2000; Azab, 2009). In addition, a recharge from deep aquifers is possible. (Lankester, 2012). The total depths vary between 12.4 m and 101 m, the diameters extend from 1 m to 2m, and the depths to water levels range from 2.10 m to 100 m, respectively (Arafat et al. 2017).

3. Materials and methods

The geophysical investigation was conducted on an area extending 40 × 50 km with a total area of approximately 505 km2. Vertical Electrical Sounding surveys were measured using Syscal Pro manufactured by IRIS Company (France). A total of 32 VESs were measured using AB/2 up to 1000 m. same number of TDEM soundings were measured in the same sites of VES with 100 x 100 m loop (Fig. 1b).

To calibrate the resistivity model with the basic information, VESs and TDEMs numbers (13, 11, 9, 23, and 27) were measured beside the boreholes (1, 2, 3, 4 and 6) respectively. The interpretation of VES was applied through two steps; first, a manual interpretation using standard curves was made, and second, the manual model was introduced into a computer program (Res1D, V1beta, 2001) to obtain the final model representing the layer parameters as resistivity and thickness (Fig. 3a). The interpretation of TDEM was done by (ZONDTEM1D, V 5.2, 2016) (Fig. 3b). The initial model was approximated from the interpreted VESs data and then compared with the logs data of previously drilled wells (Fig. 3c). The final model of VES and TDEM were collected to reach a unified model that gives a good visualization of the subsurface layers in the area under investigation and the presence and extension of the aquifer.

A total of 6 wells (Fig. 1b) served in October 2021 from existing wells corresponded to Quaternary aquifer. The samples were taken immediately from the borehole after 10 minutes of pumping the well. The Global Positioning System (GPS) was used to define well sites. (Fig. 1b). Physicochemical parameters (pH, EC, and TDS) were obtained using calibrated portable instruments at the time of water sampling. The concentrations of Ca^{2+}, Mg^{2+}, Na^{+}, K^{+}, SO_4^{2-}, and Cl^{-} were measured by A Thermo Scientific Ion chromatograph (IC, model Dionex, ICS-1100). HCO_3^{-} anion was examined titrimetrically versus sulfuric acid by neutralization method. The accuracy of the water analysis can be obtained using the charge balance error, and all of samples were within the acceptable limit (±5%).

4. Results and discussion

4.1 Geophysical Investigation

Interpretation results for both vertical electrical probes and electromagnetic probes showed the division of the subsurface layers into four layers according to their geoelectrical properties. Well logs data of drilled wells greatly helped in setting the prototype for building the interpretation. There is near agreement between the interpretations resulting from the data of vertical and electromagnetic sounding. The findings of the geoelectrical interpretation for TDEMs and VESs (Nos. 13, 11, 9, 23, and 27) measured nearby boreholes Nos (1, 2, 3, 4 and 6) reveal an agreeable resemblance for the outcomes of the boreholes data (Fig.1b). An example of the correlation between the interpretation of TDEM and VES Nos. (13)

and the lithological description for the borehole logs No. (1) is shown in Figure (3). The results of the geoelectrical interpretation indicate the subsurface cross-section that comprises different geoelectrical layers. Two cross-sections represented in Figure (4 a, b).

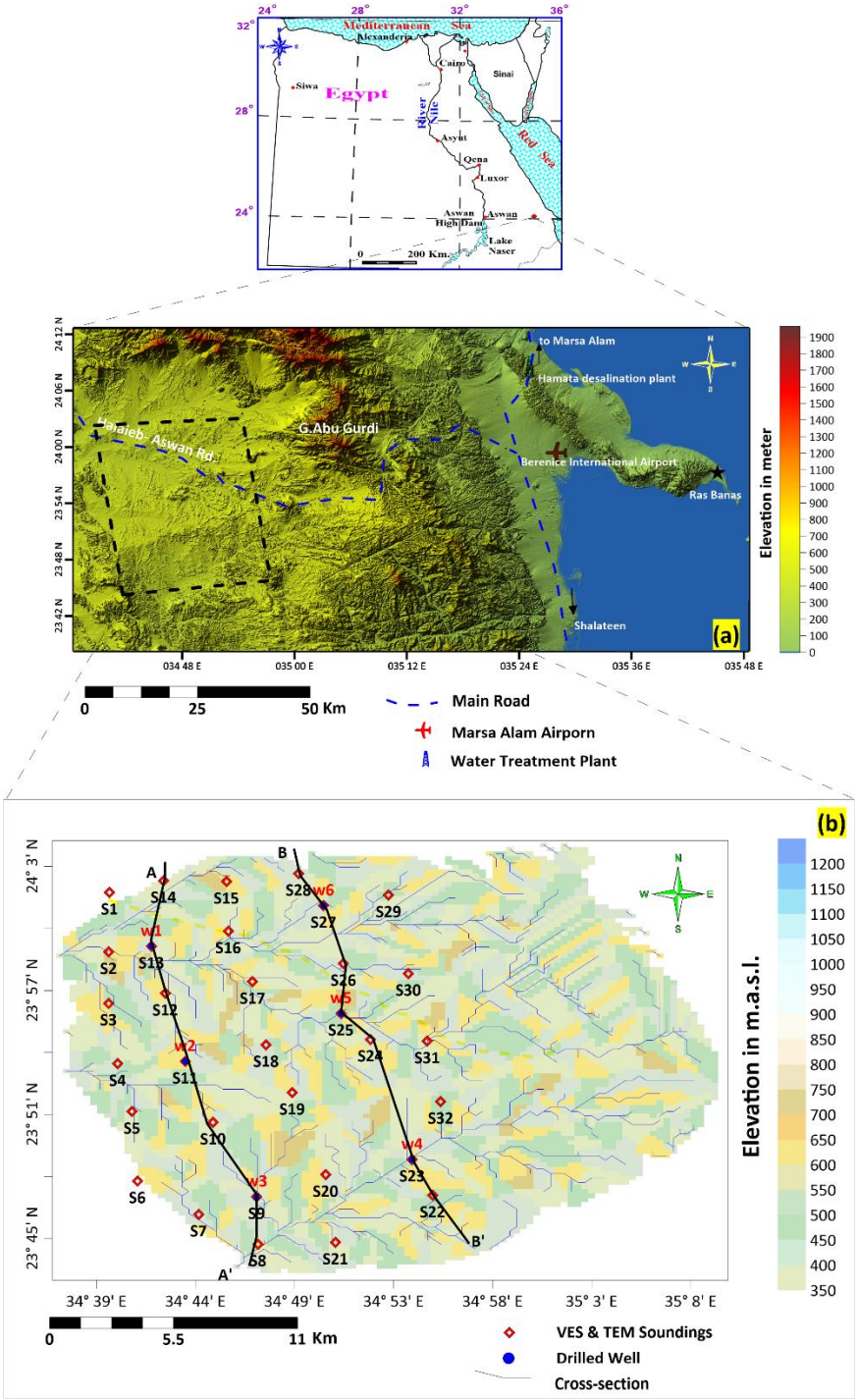

Fig. 1 Location map of the study area.

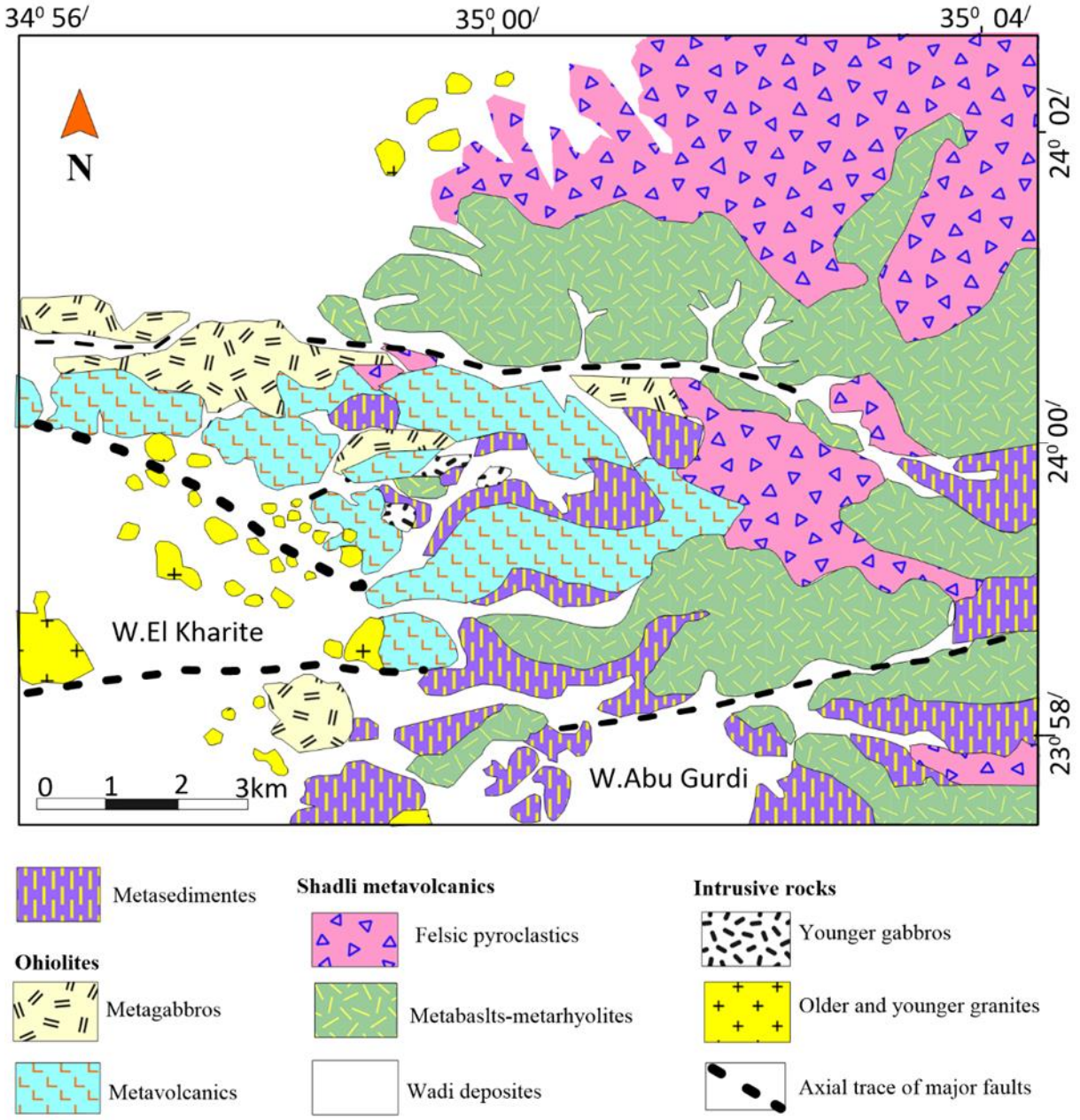

Fig. 2 Geologic map of study area (Abd Allah, 2012).

Table 1. The description of the geoelectrical layers with its elevations, depths, and the range of its resistivity values.

Geoelectrical layers	Elevation in meter above sea level (amsl)		Thickness in meter		Resistivity value in Ohm.m	
	Min	Max.	Min	Max.	Min	Max.
Surface Layer	410	511	53.69	86	2732	4376
Second Layer (Freshwater aquifer)	356	444	16	27	32	55
Third Layer	333	416	106	158	11	17
Fourth Layer	206	265	unlimited		4246	4600

Table 2. Statistical overview of the hydrochemical variables (n=6) for analyzed samples.

Parameters	Units	Minimum	Maximum	Mean	SD
pH	-	7.60	8.40	8.17	0.28
EC	µS/cm	1650.00	2340.80	2041.97	273.22
TDS	mg/l	1036.00	1501.00	1208.17	176.00
Na^+	mg/l	54.10	270.00	151.93	68.23
Ca^{2+}	mg/l	80.00	170.80	110.40	32.39
Mg^{2+}	mg/l	26.30	97.30	73.63	27.62
K^+	mg/l	3.90	13.20	6.20	3.20
Cl^-	mg/l	202.50	636.20	361.37	170.08
SO_4^{2-}	mg/l	188.00	320.00	253.48	41.09
HCO_3^-	mg/l	100.00	183.00	156.41	26.92
CO_3^{2-}	mg/l	4.80	18.00	10.48	4.19
TH	mg/l	363.58	697.33	577.90	104.04

EC= Electric Conductivity, TDS=Total Dissolved Solid and TH=Total Hardness

The first geoelectrical layer consists of Wadi deposits composed of gravel, flint, silt, and sand “Holocene” of Quaternary deposits. The second geoelectrical layer contents of loose sand of Quaternary deposits with fresh groundwater. The third geoelectrical layer comprises sandy shale. The fourth geoelectrical layer comprises basement intrusion. The lower surface of this layer is not detected at any TDEM and VES (Fig. 3 and Fig. 4). A description example of the subsurface stratigraphy for the borehole No. 1 is shown in Figure (3 c). Table (1) shows the description of the geoelectrical layer with its elevations, depths, and the range of its resistivity values. The water-bearing formation were obtained from the lithological description of the borehole logs of natural gamma logs, electrical resistivity logs in wells nos. (1, 2, 3, 4 and 6). The distribution of thickness and elevation of the aquifer (second geoelectrical layer) represented in figure (5 a, b), The western part of the area under investigation represented the first promising priority zone for planning drilling boreholes. (From Fig. 5 b the zone of VESes 5, 6, 10, 18,19, 30,31 and 29) from geophysical study.

4.2 Physicochemical characteristics of groundwater

The descriptive statistics of the groundwater chemical data mentioned in Table 2 and Figure .6. The relative cornucopia of the major ions is as follows: $Na^+ > Ca^{2+} > Mg^{2+} > K^+$ whereas $Cl^- > SO_4^{2-} > HCO_3^-$. The pH value of groundwater samples ranges from 7.60 to 8.40 with an average about 8.17 and standard deviation about 0.28. Generally, pH of the groundwater samples was observed to be alkaline in nature. The electrical conductivity at 25 0C varies between 1650.00 and 2340.80 µS/cm with an average about 2041.97. Based on EC, water classification of the groundwater samples represents weakly (50%) to moderately (50 %) mineralized water (Table. 3).

According to TDS, water classification shows that all of groundwater samples are classified as slightly brackish water category (Table 4). Spatial distributions EC and TDS and other parameters are demonstrated in maps (Figs 7. a-h). These maps revealed that concentrations rise from the northeast to the southeast with groundwater flow direction (Fig.5a) of the area under investigation, with the exception of bicarbonate, which moves in the opposite direction when compared to other parameters.

4.3 Hydrochemical facies and groundwater classification

Piper plot (Piper 1994) is commonly used to assess the characteristic chemical composition of aquifer system. The majority of the groundwater samples, the alkaline earth elements ($Ca^{2+} + Mg^{2+}$) exceeded the alkali earth elements ($Na^+ + K^+$). Two hydrochemical facies could be identified on the diagram. The Ca + Mg-Cl + SO_4 type (facies 5) consisting of three samples (Fig. 8a). In these facies, the primary hydrogeochemical processes are gypsum/anhydrite dissolution and reverse ion exchange. (Alharbi and Zaidi 2018). The remaining 3 samples belong to the mixed Ca + Mg − Cl + SO_4 type (Facies 4). Generally, Dominance of Ca^{2+} and Mg^{2+} indicate that the water mineralization is affected by the reverse ion exchange process.

Instead of using the traditional Piper ternary diagram, Matthes (1982) advocated classifying groundwater sources using the values of the Base Exchange Index (r1). Eq. (1) is used to compute the Base Exchange Index (r1). If r1 < 1, the origin of the groundwater is depicted as $Na^+ - SO_4^{2-}$, whiles r1 > 1 indicates that the water is of Na^+ - HCO_3^- type.

Base−exchange index (r1)=$(Na^+ - Cl^-)/SO_4^2$ (concentration in meq/l) **(1)**

Table 3. Water classification based on electrical conductivity (Detay and Carpenter 1997)

Electrical conductivity (µS/cm)	Mineralization	Number of samples	% of samples
<1000	Very weakly mineralized water	-	-
1000–2000	Weakly mineralized water	3	50
2000–4000	Slightly mineralized water	3	50
4000–6000	Moderately mineralized water	-	-
6000–10,000	Highly mineralized water	-	-
>10,000	Excessively mineralized water	-	-

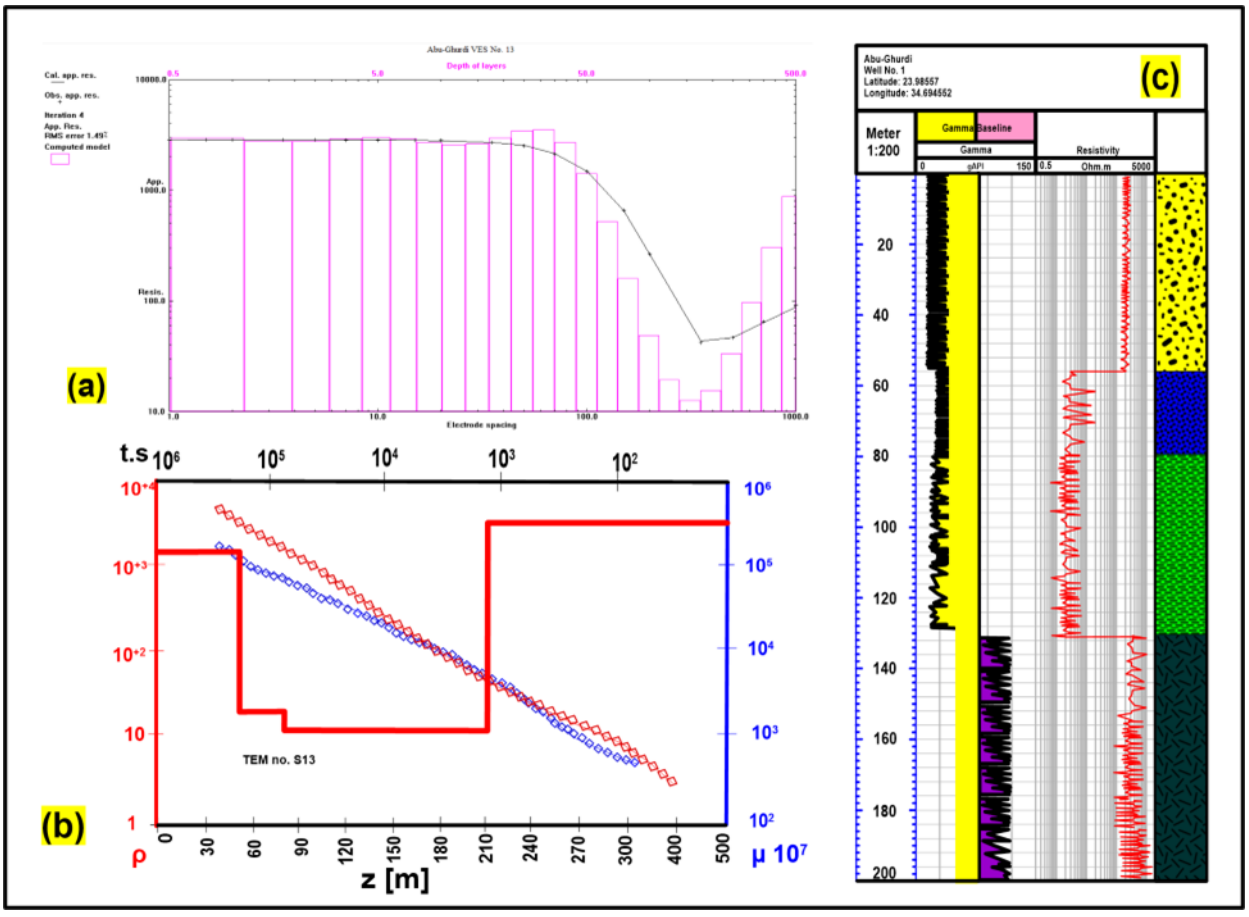

Fig. 3 (a) 1-D model inversion examples of the VES stations (S13), (b) 1-D model inversion examples of the TEM stations (S13), (c) well logging charts (resistivity and gamma rays) and lithological design of wells W1.

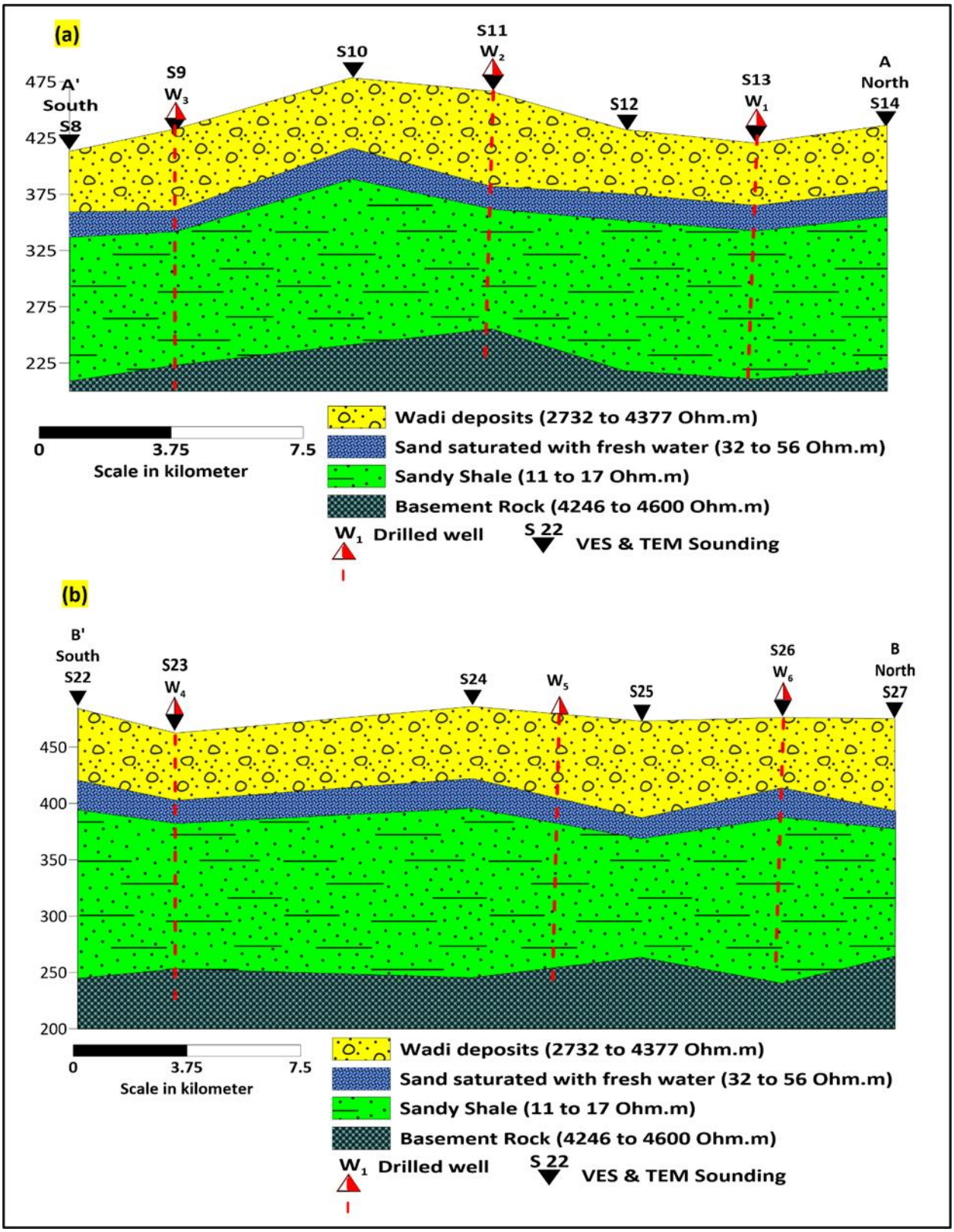

Fig. 4 (a) Geoelectric cross-section A-A/, (b) Geoelectric cross-section B-B/.

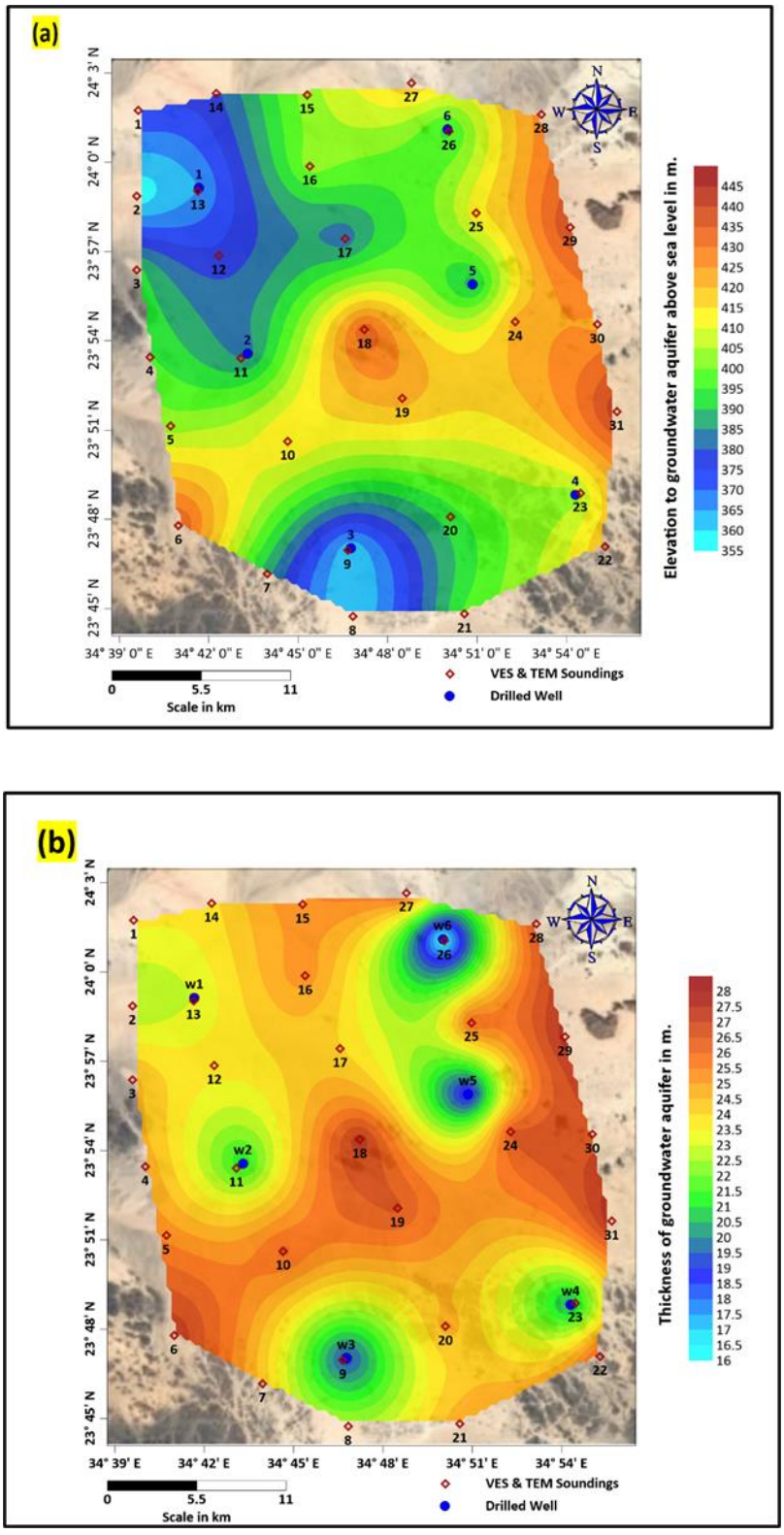

Fig. 5 (a) Elevation contour map of groundwater aquifer, (b) thickness contour map of groundwater aquifer.

Table 4. Classification of groundwater according to the TDS (mg/l).

	TDS	Water class	Number of samples	% of samples
According to Freeze and Cherry (1979)	<1000	Fresh water type	-	
	1000–10,000	Brackish water type	6	100
	10,000–100,000	Saline water type	-	
	>100,000	Brine water type	-	-
According to Todd (1980)	10–1000	Fresh water	-	
	1000–10,000	Slightly-Brackish water	6	100
	10,000–100,000	Brackish water	-	-
	>100,000	Brine water	-	-

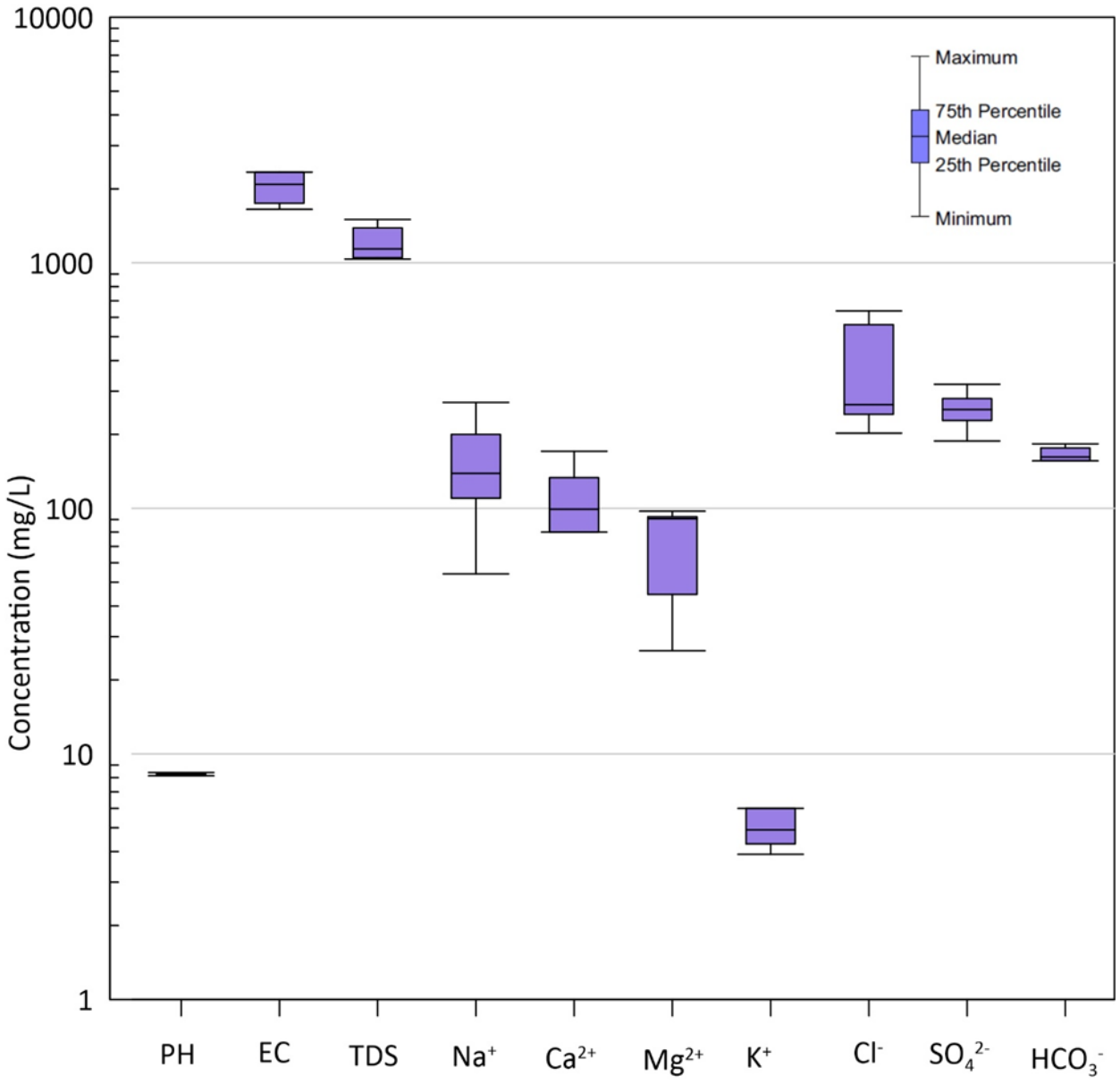

Fig. 6 Box plots showing water chemistry of the quaternary aquifer.

Figure. 8c demonstrates that all of the water samples had r1> 1, indicating a high preference for the Na-SO_4 type, which is associated with salinization (Stuyfzand 1986). Calculating the Na/Cl ratio that was subsequently utilized to determine the magnitude of ion exchange in water chemistry, supported this. The Na/Cl ratio ranged from 0.35 to 1.05 meq/l, with an average of 0.68 meq/l (Table 5). Because of the predominance of Cl^- in the water as NaCl, the calculated results revealed that 83 percent of groundwater samples had a Na/Cl ratio smaller than unity. The elevated Cl^- levels could be attributable to base-exchange mechanisms or the leaching of marine salt facies (Abdalla et al. 2020). The Na/Cl ratio was more than unity in the remaining samples (17%), implying the emission of Na^+ from silicate weathering during rock-water contact, evapotranspiration and the meteoric origin of the groundwater (Abdalla et al. 2020).

The groundwater has been categorized too based on meteoric genesis index (r2) which was calculated using Eq. (2).

Meteoric genesis index (r2) = $(K^+ + Na^+) - Cl^- / SO_4^{2-}$ (in meq/l) **(2)**

The values of r2 are <1, indicates that groundwater is of deep or extreme meteoric percolation type and r2 >1 distinct groundwater source belongs to shallow or light meteoric percolation type (Matthes, 1982). The analyzed groundwater samples in area under investigation show that all of groundwater samples belong to deep meteoric percolation type (r2<1) meaning that groundwater samples had longer residence time via deeper percolation (Fig. 8c).

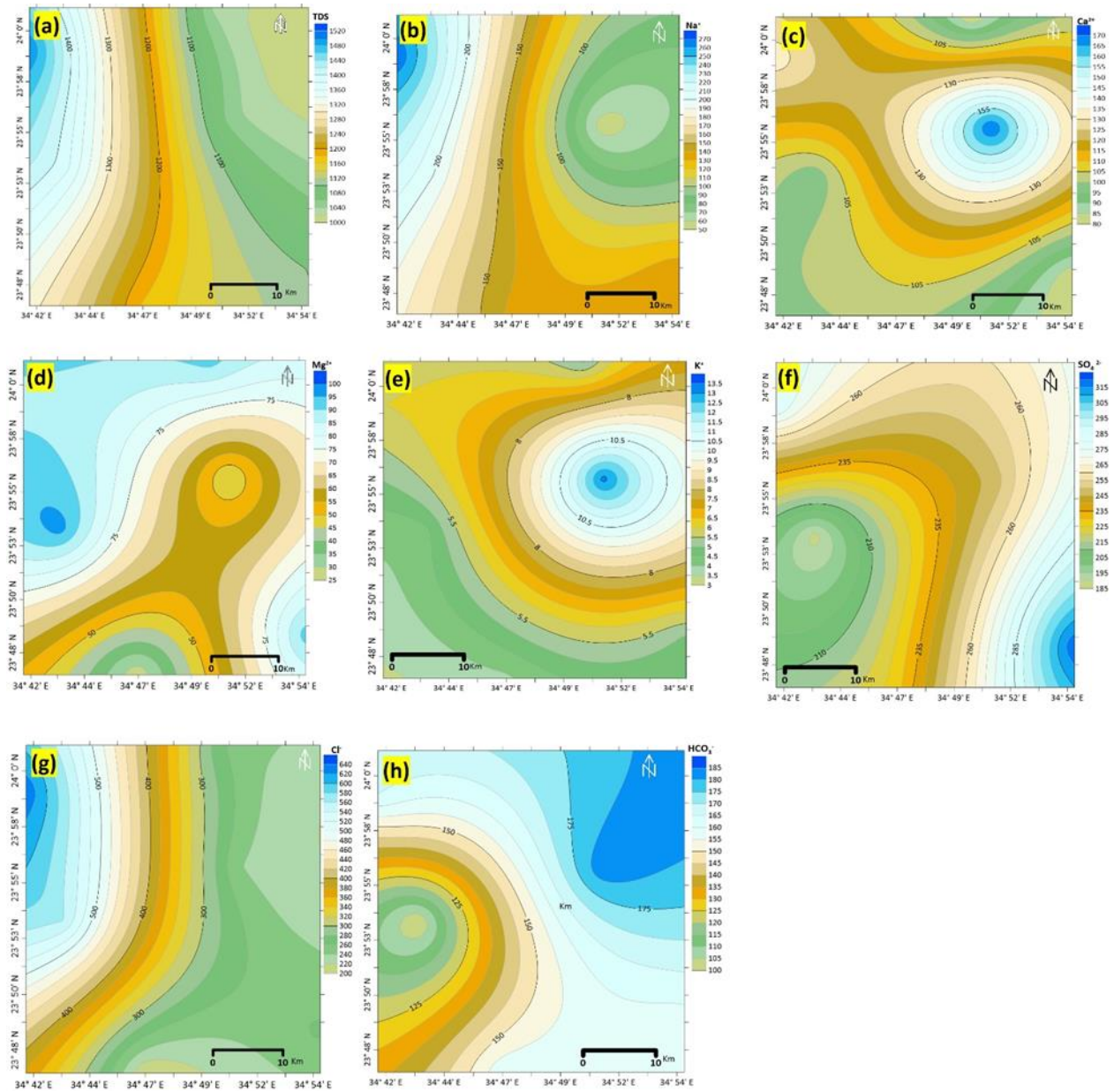

Fig. 7 Spatial distribution maps for physicochemical parameters of the quaternary aquifer. **(a)** TDS distribution map **(b)** Na^+ distribution map **(c)** Ca^{2+} distribution map **(d)** Mg^{2+} distribution map **(e)** K^+ distribution map **(f)** $SO4^{2-}$ distribution map **(g)** Cl^- distribution map **(h)** HCO_3^- distribution map.

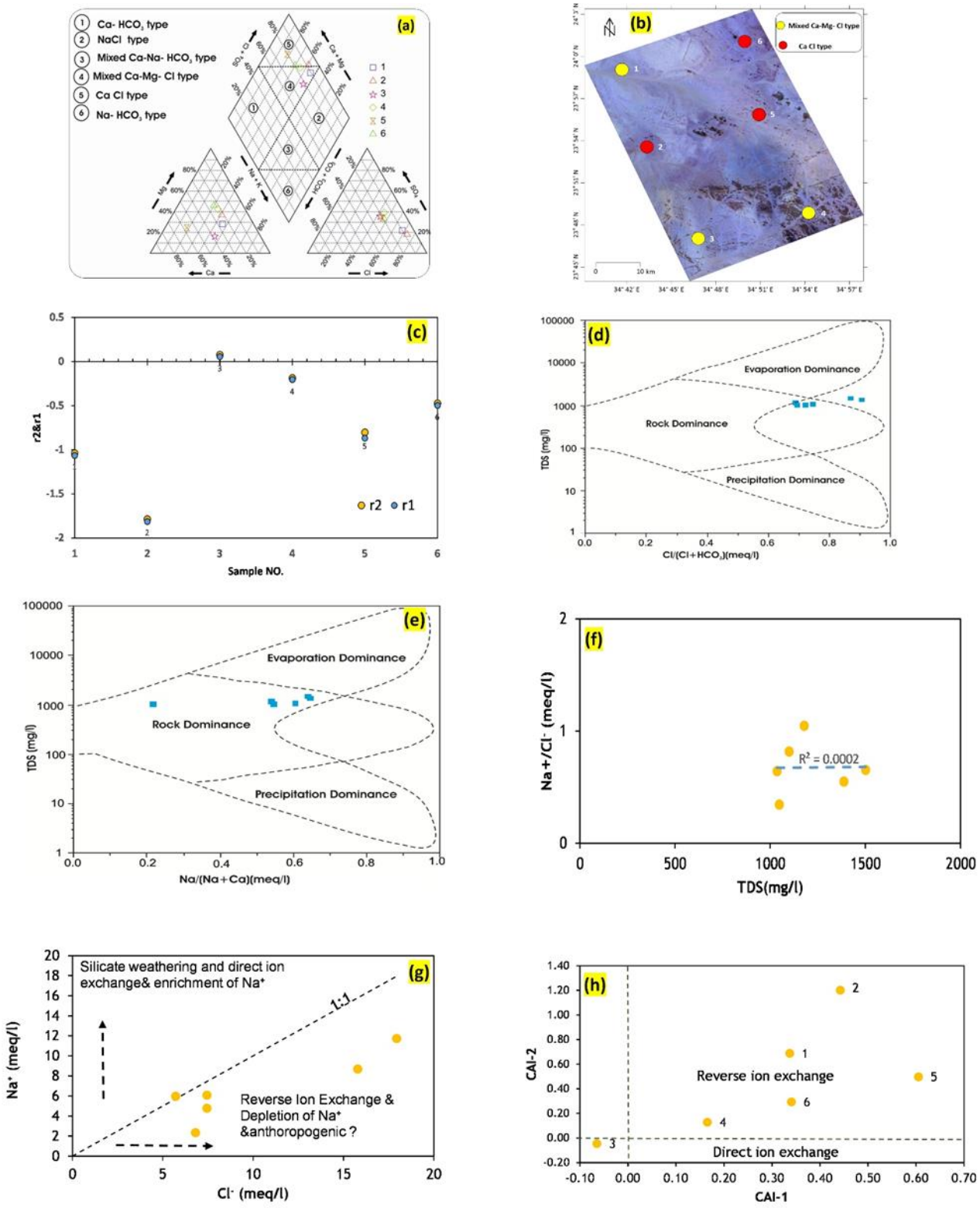

Fig. 8 (a) Piper diagram of groundwater samples from the quaternary aquifer **(b)** spatial distribution map of hydrochemical facies **(c)** base exchange index (r1) and meteoric genesis index (r2) of the groundwater samples **(d)** and **(e)** Gibbs diagrams for controlling factor of groundwater quality **(f)** TDS vs Na/Cl. **(g)** Plot of a Na^+ vs. Cl^- **(h)** CAIs indicating base ion exchange processes in groundwater.

Table 5. Ratios of ion exchange reaction and silicate weathering in the study area.

Parameter	Minimum	Maximum	Average
Na/(Na + Ca)	0.22	0.64	0.53
CAI 1	-0.06	0.61	0.30
CAI2	-0.05	1.20	0.46
Cl/ΣAnions	0.42	0.73	0.53
Mg/(Ca + Mg	0.30	0.66	0.51
Na/Cl	0.35	1.05	0.68
r1	-1.81	0.06	-0.73
r2	-1.79	0.08	-0.70
RI	1.79	8.29	3.84

Revelle (1941) proposed the equation for calculating the Revelle Index (RI) which is used to assess groundwater salinization Eq. (3)

Revelle index (RI) = Cl^- / (HCO_3^- + CO_3^{2-}) (concentration in meq/l) **(3)**

When RI is less than 0.5, there is no salinization; when RI is between 0.5 and 6.6, the groundwater is somewhat affected; and when RI is larger than 6.6, the groundwater is severely damaged, according to Revelle 1941. In current study the RI ranged from 1.79 to 8.29 with average 3.84 (Table 5). Indicating that about all the groundwater samples with RI values >0.5 is affected by salinization. The sources in charge of a high level of salinization were further assessed by geochemical assessment.

The Gibbs diagram can are commonly used to depict natural process that controlling the chemical composition of groundwater such as evaporation, rockwater interaction and rainfall (Kumar 2016). Gibbs plots for groundwater samples in area under investigation indicated that evaporation is the prime action controlling chemistry of the shallow groundwater with minimal effect of rockwater interaction in the aquifer (Figs. 8d and e). The scatter plot of TDS vs Na^+/Cl^- clearly confirms the influence of evaporation on groundwater. TDS concentrations in groundwater are increasing while the Na^+/Cl^- ratio remains constant, is an index of an evaporation predominant environment. Figure .8f exhibits a horizontal trend line (r=0.01), implying that evaporation is a frequent geochemical process that regulates groundwater chemistry (Rajimohan and Elango 2004; Embaby and Ali 2021).

Ion exchange occurring in the aquifer was investigated by scatter diagrams of Na^+ vs Cl^- ions. The studied samples characterized by the enrichment of Cl^- concentrations with respect to Na^+ and have Na^+/Cl^- ratios less than unity (83% of samples) (Fig. 8g). It's possible that the excess Cl^- in ground water came from sources other than halite dissolution. The removal of Na^+ from groundwater due to reverse ion exchange may have modified the Na^+/Cl^- ratio (Zaidi et al. 2015b).

Scholler (1965) suggested two Chloro-Alkaline Indices CAI1 and CAI2 for interpretation the ion exchange process throw rock water interaction. It is calculated by Eq.(4) and (5), where all ions are stated in in meq/l.

$CAI1 = (Cl^- (Na^+ + K^+) / Cl)$ **(4)**

$CAI2 = (Cl^- (Na^+ + K^+)/(SO_4^{2-} + HCO_3^- + CO_3^{2-} + NO_3^-)$ **(5)**

A positive value of CAI1 implies reverse ion exchange of Na+ and K+ from the groundwater with Ca2+ and Mg2+ from the aquifer matrix, while a negative index informs that there is cation exchange taking place between Ca2+ and Mg2+ in the groundwater and Na+ and K+ in the host environment. The indices of CAI1 and CAI2 estimated for samples showed about 83% groundwater samples were positive, Indicating reverse ion exchange process. Only one sample (17%) had negative values of CAI1 and 2 indicated a direct ion exchange process (Fig.8h).

Furthermore, a plot of Ca^{2+} + Mg^{2+} versus HCO_3^- + SO_4^{2-} demonstrates the dominance of ion exchange reactions, particularly reverse ion exchange in the aquifer as (76%) of samples shift to the left due to an excess of Ca^{2+} and Mg^{2+} over + HCO_3^- + SO_4^{2-} (McLean and Jankowski, 2000) (Fig.9a). The scatter plot of Ca^{2+} + Mg^{2+} versus Na^+ + K^+ indicates all the points fall above equiline infers the dominancy of Ca^{2+} + Mg^{2+} and reverse -ion exchanges process is dominant (Fig. 9b).

To identify the effect of silicate weathering, the ratios of Cl/Σ anions, Na^+/Cl^- , $Na^+/ (Na^+ + Ca^{2+})$ and $Mg^{2+}/(Ca^{2+} + Mg^{2+})$ have been employed. (Naseem et al. 2010; Kumar et al. 2018). The <1 value of Cl/Σ anions is pointer of silicate mineral weathering (Kumar et al. 2018) in the area under investigation (Table 5). This is endorsed by the <1 values of $Na^+/ (Na^+ + Ca^{2+})$ and $Mg^{2+}/ (Ca^{2+} + Mg^{2+})$ (Table 5).

Groundwater samples fell between 1:2 (Ca^{2+} +Mg^{2+} = 0.5 TZ+) line and 1:1 equil-line in a scatter plot of Ca^{2+} + Mg^{2+} vs. total cations (TZ+) showing that some of these ions (Ca^{2+} + Mg^{2+}) are came out from the weathering of silicate minerals (Fig. 9c) (Hwang et al., 2017).

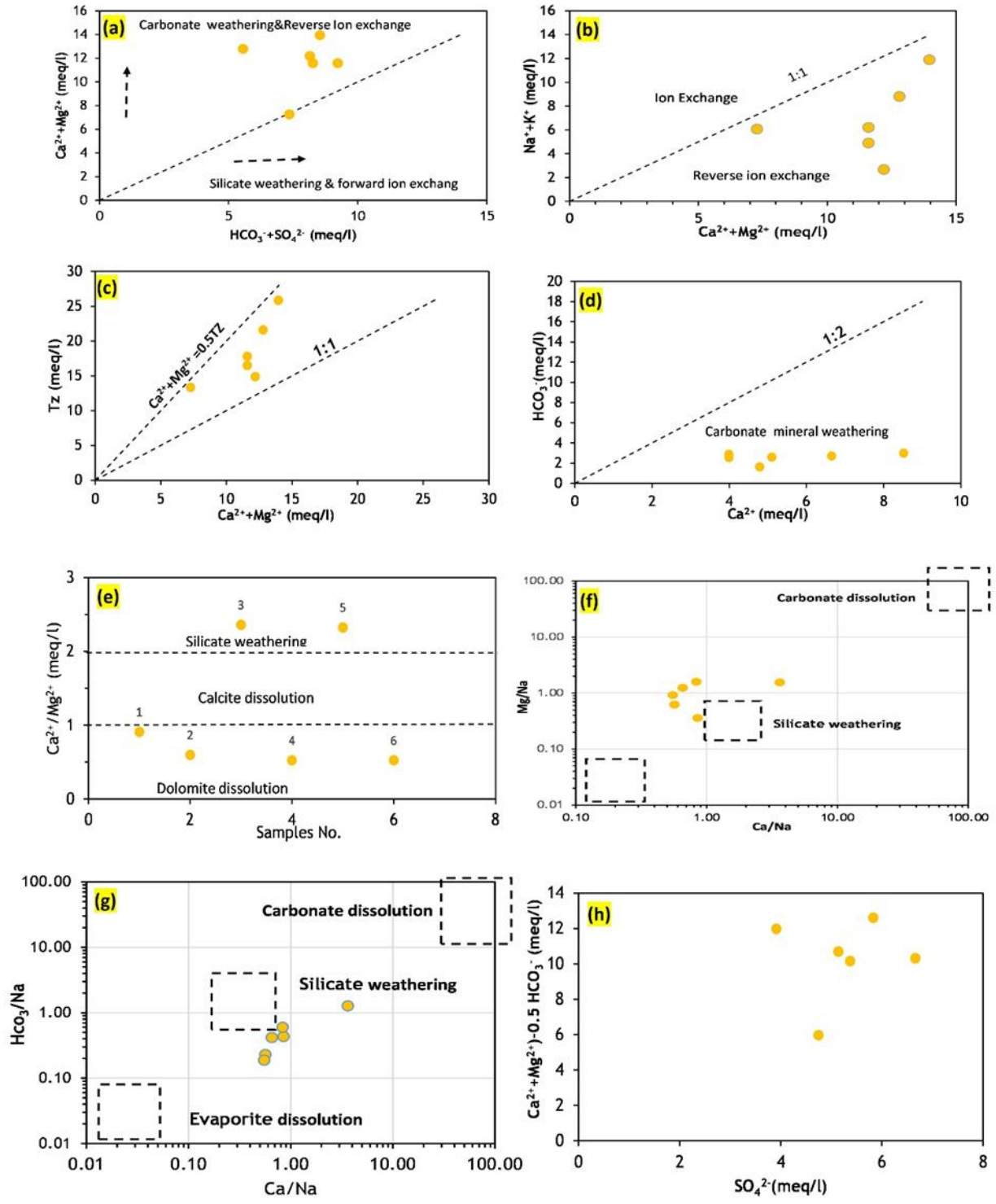

Fig. 9 Ions scatter diagram indicating various hydrogeochemical processes of groundwater in the study area.

On groundwater chemistry, the important effect of silicate weathering could be specified by the bivariate schemes of Ca^{2+} + Mg^{2+} over HCO_3^- + SO_4^{2-}. The dominance of Ca^{2+} + Mg^{2+} over HCO_3^- + SO_4^{2-}indicates carbonate weathering, whereas, the abundance of HCO_3^- + SO_4^{2-} reflect silicate weathering as the primary process of ion exchange (Papazotos et al. 2019). Figure. 9a shows that the bulk of samples (76%) were above and along the equiline, indicating that carbonate weathering is the primary geochemical mechanism causing increased HCO_3^- and SO_4^{2-} concentrations in groundwater (Datta and Tyagi, 1996). The bivariate plot of Ca^{2+} vs HCO_3^- showed that most of the samples fall below the 1:2 line indicating

calcium and bicarbonate are related to calcite weathering (Mthembu et al. 2020) (Fig. 9d).

The Ca^{2+}/Mg^{2+} molar ratio signifies calcite and dolomite dissolution in groundwater. $Ca^{2+}/Mg^{2+}=1$ demonstrates dolomite dissolution, $1< Ca^{2+}/Mg^{2+}<2$ signifies calcite dissolution, and $Ca^{2+}/Mg^{2+} > 2$ indicates silicate dissolution (Paul et al., 2019 and Brindha et al., 2017). Figure. 9e shows most of the samples in the area under investigation had Ca^{2+}/Mg^{2+} ratio less than 1(67%) and between 1 and 2(33%), revealing that dolomite and calcite dissolution provided towards high Ca^{2+} and Mg^{2+} followed by dissolution of silicate mineral. End-member diagrams have been constructed for further analysis of rock types concerned within the rock weathering processes operating groundwater hydrochemistry (Gaillardet et al. 1999). The bivariate plots Ca^{2+}/Na^{+} versus Mg^{2+}/Na^{+} and Ca^{2+}/Na^{+} versus Na^{+}/HCO_3^{-} are used to classify three important processes that govern the geochemistry of water i.e., carbonate dissolution, evaporite dissolution, and silicate weathering (Mukherjee and Fryar, 2009). As shown in Figures 9f and g, most of the samples are mainly reflecting that water were influenced by silicate weathering and evaporates dissolution process.

The groundwater of the area under investigation has a high content of SO_4^{2-}. This SO_4^{2-} enhancement could be related to gypsum weathering. The binary plot of $Ca^{2+} + Mg^{2+} - 0.5\ HCO_3^{-}$ against SO_4^{2-} (Fig. 9h) demonstrated that all the sampling points over the zero value validated the effects of gypsum weathering in the aquifer system (Karunanidhi et al., 2021).

4.4 Quality criteria for drinking water supply and irrigation

4.4.1 Drinking water quality

To obtain an assessment of the suitability of groundwater as potable or drinking water, the method of calculating the concentration of species chemistry in samples taken from groundwater can be used and compared with the standard values of the World Health Organization (WHO 2011) drinking guidelines. Table 6 and Figures (10 a-h) show the hydro-chemical parameters of the area under investigation compared to standard values of WHO (2011).

Total hardness (TH) and total dissolved solids (TDS) are two basic and influential parameters in evaluating drinking water quality. The TDS concentration in all groundwater samples in area under investigation varies between 1036.00 and 1501 mg/l, it is a little higher than the threshold limit of drinking water (1000 mg/L). The groundwater samples collected in the area under investigation have TH values range from 363.58 to 697. As shown in Figure .11a, obviously, groundwater samples of area under investigation (83.33 %) were mainly in the very hard brackish category (TH >450 mg/l).

Table 6. The hydro chemical parameters of the study area in comparison with WHO (2011) drinking water Standard.

Parameters (units)	WHO (2011)	Number of samples exceeding desirable limits	Percentage of samples
pH	6.5 – 8.5	-	-
Ca^{2+} (mg/L)	75	6	100
Mg^{2+}(mg/L)	100	-	-
Na^{+} (mg/L)	200	1	16.66
K^{+} (mg/L)	10	1	16.66
Cl^{-} (mg/L)	250	4	66.66
SO_4^{2-} (mg/L)	250	3	50
TDS (mg/L)	1000	6	100

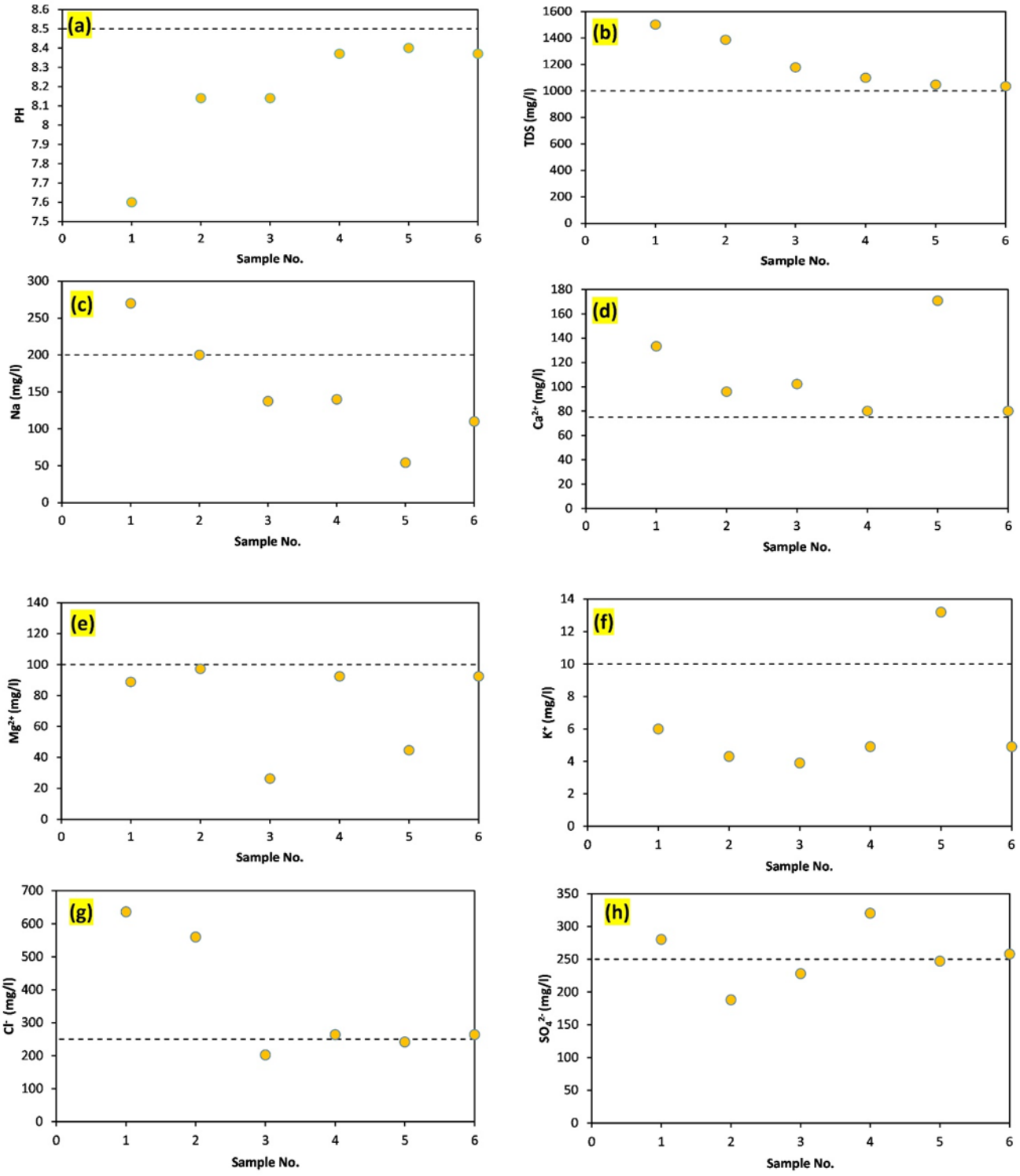

Fig. 10 Comparison of drinking-quality groundwater with the WHO recommended limit (dash line).

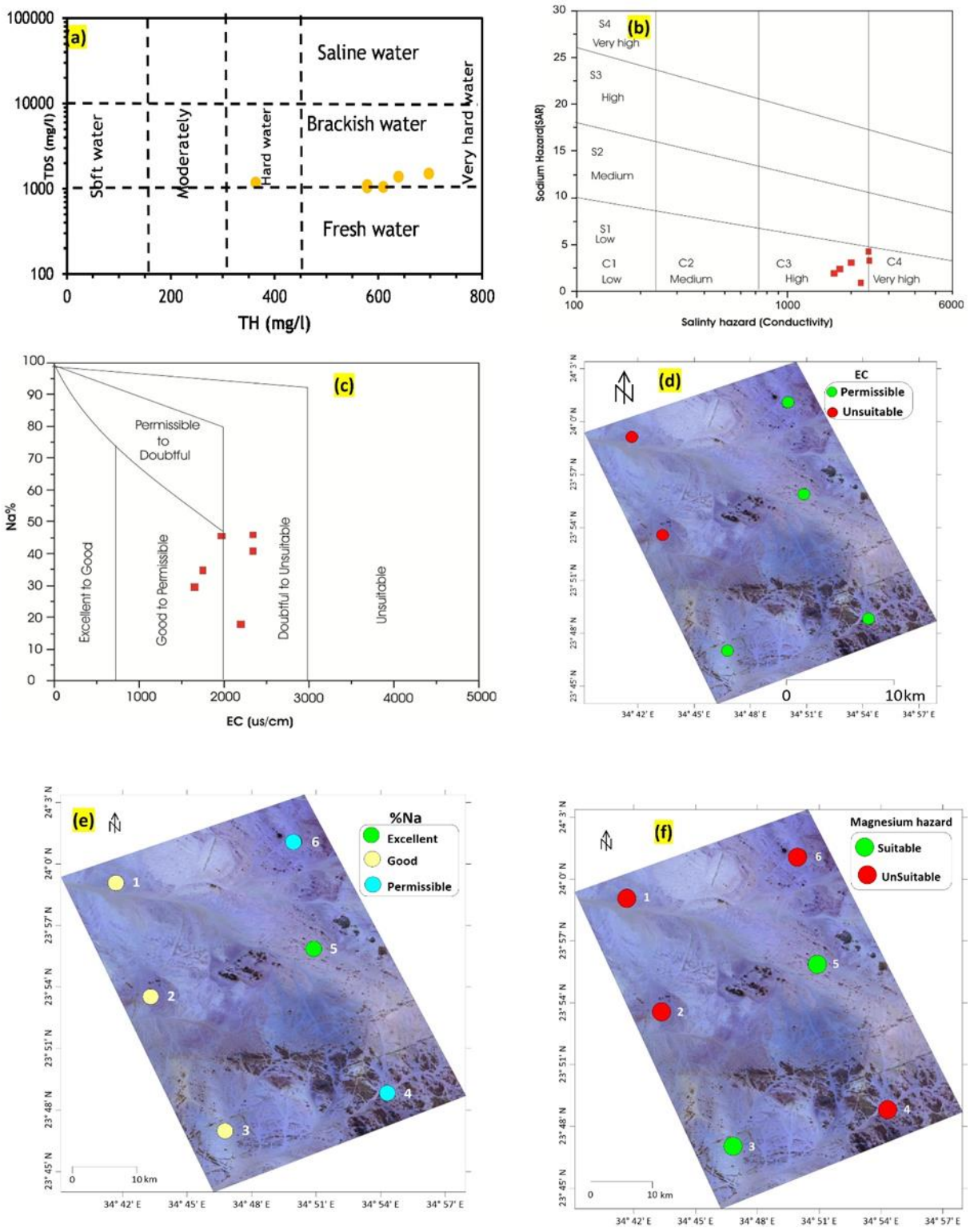

Fig. 11 (a) Scatter plots TDS vs. TH showing groundwater quality **(b)** USSL Groundwater salinity hazard diagram **(c)** Wilcox diagram **(d)** Spatial distribution of salinity hazard based on EC **(e)** Spatial distribution of %Na **(f)** Spatial distribution of Magnesium hazard (MH).

4.4.2 Irrigation water quality assessment

The following criteria were used to gauge the quality of groundwater for agricultural purpose: salinity hazard (EC), sodium adsorption ratio (SAR), soluble sodium percentage (SSP), permeability index (PI) and magnesium hazard (MH). All the concentrations for these criteria measured in meq/l unit (Table 7).

Salinity hazard is assessed by electrical conductivity and total dissolved solids. Commonly, water with a TDS of about 5,000 mg/l is incompatible for irrigation (Pillsbury and Blaney 1966; Ayers and Westcot 1985). After analysis, The EC values of groundwater samples varied from 1650.00 to 2340.80 µS/cm with mean value 2041.97 µS/cm. the US Salinity Laboratory Staff (1954) divides water into four classes based on the EC in µS/cm (Table 8). As shown in table 7, about 66.66 % (n=4) of the studied groundwater samples from the area under investigation were acceptable for irrigation with EC ≤ 2250 µS/cm, this is indicating that groundwater in the area under investigation is appropriate for irrigation. The rest of the samples were inappropriate for irrigation purposes.

The sodium adsorption ratio (SAR) is a criterion for evaluating whether water is suitable for agricultural irrigation. Eq. (6) can be used to express the SAR.

$$SAR = \frac{Na^{+}}{\sqrt{\frac{Ca^{2+} + Mg^{2+}}{2}}} \quad \textbf{(6)}$$

The computed SAR values in the research area are presented in Table .8 The calculated values of SAR in the area under investigation vary between 0.95 and 4.45 with an average 2.75 (Table 8). All samples locate under (no problem) category consistent with the proposed water classification for SAR with values < 10 and can be used safely for all types of soil. The relationship between SAR and EC were drawn on the US salinity diagram (Richards, 1954) and it was observed that 67% (n=4) of the samples locate in the field of C3–S1 category (Fig. 11b). It indicates that these water samples have low alkalinity and high salinity risk, it can be utilized for irrigation purpose in all soil types with low risk of sodium exchange. Remaining 33% % of the samples lie in C4–S1 class, this shows low alkalinity content and very high salinity. So, these groundwater samples are appropriate for plants that having good salt tolerance but inappropriate for irrigation in soils with limited drainage.

Table 7. Water quality parameters for irrigation purposes

Classification	Categories	Ranges	No. of samples	% samples
EC (Wilcox 1955)	Excellent	<250	n=0	0
	Good	250–750	n=0	0
	Permissible	750–2250	n=4	66.66
	Doubtful	2250–5000	n=2	33.34
	Unsuitable	>5000	n=0	0
SAR (Richards, 1954)	Excellent	0-10	n=6	100
	Good	10-18	n=0	0
	Doubtful	18-26	n=0	0
	Unsuitable	>26	n=0	0
Na % (Wilcox, 1955)	Excellent	0-20	n=1	16.66
	Good	20-40	n=2	33.33
	Permissible	40-60	n=3	49.99
	Doubtful	60-80	n=0	0
	Unsuitable	80-100	n=	0
RSC (Richards, 1954)	Good	<1.25	n=6	100
	Medium	1.25-2.5	n=0	0
	bad	>2.5	n=0	0
PI (Doneen, 1962)	Unsuitable	0–25	n=0	
	Good	25–75	n=6	100
	Excellent	≥75	n=0	
Mg^{2+} hazard (mg/l) Paliwal (1972)	Suitable	<50	2	33
	Unsuitable	>50	4	67

Table 8. Statistical Summary of Computed Water Quality Parameters for Irrigation.

TH	363.58	697.33	577.90
SAR	0.95	4.45	2.75
Na%	18.08	46.02	35.84
MAR	29.77	65.57	50.99
PI	29.72	57.63	45.05
RSC	-10.99	-4.07	-8.66

Furthermore, the percent sodium (%Na) is commonly used for assessing the appropriateness of water quality for irrigation (Wilcox 1955). %Na is calculated using Eq. (7) (Wilcox 1955).

$$\%Na = \left(\frac{Na^{+} + K^{+}}{Na^{+} + K^{+} + Ca^{2+} + Mg^{2+}}\right) x100 \quad \textbf{(7)}$$

In the area under investigated, %Na varies between 18.08 % and 46.02 % with an average 35.84 %. In the groundwater samples, the calculated values of sodium percentage reveal that the groundwater samples equally distributed between two categories, Good to Permissible and doubtful unsuitable class (Fig. 11c).

Permeability index (PI) is usually applied to evaluate how simply water flows through a soil texture. The following Eq. (8) is used to compute PI (Doneen 1964).

$$PI = \frac{Na^{+} + \sqrt{HCO_3^{-}}}{Na^{+} + Ca^{2+} + Mg^{2+}} x100 \quad \textbf{(8)}$$

All groundwater samples fall into the excellent category based on the PI values and PI classification (Table 7).

Magnesium hazard ratio (MH) is a term used in the natural water system to describe how elevated magnesium levels affect irrigation water (Szabolcs and Darab 1964; Todd 1980). It is calculated using the Eq. (9), with the concentrations measured in meq/l unit.

$$MH = Mg^{2+} / (Mg^{2+} + Ca^{2+}) \times 100 \quad \textbf{(9)}$$

In the current research, magnesium hazard values are ranges from 29.77 and 65.57 with an average value of 50.99, and only 33% of the samples are considered appropriate for irrigation purpose (Table 7).

The residual sodium carbonate (RSC) is utilized to detect carbonate groundwater on the soil and the hazard impacts of high bicarbonate. RSC is calculated using Eq. (10)

$$RSC = (HCO_3^{-} + CO_3^{2-}) - (Ca^{2+} + Mg^{2+}) \quad \textbf{(10)}$$

RSC levels of less than 1.25 meq/l are considered safe for irrigation, whereas those of more than 1.25 meq/l are considered unsafe. In the area under investigation, the calculated RSC values vary between -10.99 and -4.07 meq/l with an average value of -8.66, this indicates that all the groundwater samples were deemed safe for irrigation.

Overall, the irrigation water quality of the region under investigation is in a quite appropriate condition. Generally, the spatial distribution map of groundwater appropriateness for irrigation reveals that groundwater from the majority wells is appropriate for irrigation uses (Figs. 11 d-f).

Conclusion

The main source of groundwater recharge in the area under investigation is rain. The total net recharge of groundwater in the area under investigation was less than150 mm/year in the area under investigation.

The geophysical interpretation indicated that the subsurface layers include four geoelectrical layers consisting of valley sediments, fine sands containing fresh water, sandy clay and basement rocks, respectively. The studied area contains a shallow freshwater aquifer, belonging to Quaternary aquifer. The Quaternary aquifer represents an important source of fresh water in the area under investigation.

Six groundwater samples were gathered and analyzed for diverse hydrogeochemical parameters to comprehend hydrogeochemical characteristics, major hydrogeochemical processes that govern groundwater chemistry, quality and suitability assessment for drinking and irrigation uses from six wells of shallow quaternary aquifer in southern part of Eastern Desert, Egypt.

Most groundwater samples are related to the freshwater type, with water salinity ranging from 1036 to 1501 mg/L. According to TH Classification, all samples belong to the category of very hard water. Dominant hydrogeochemical facies observed in this area is Ca + Mg-Cl + SO_4 and mixed Ca + Mg − Cl + SO_4 type. According to Base Exchange index (r1) and (r2), the water classified as Na-SO4 type, which is associated with salinization (r1<1) and deep meteoric percolation type (r2<1) meaning that they had longer residence time via deeper percolation.

The groundwater chemistry depends on reverse ion exchange weathering of carbonate minerals as well as silicate weathering. Moreover, evaporation process controlling factors of groundwater chemistry of groundwater in quaternary aquifer. Results from EC, sodium adsorption ratio (SAR), soluble sodium percentage (SSP), permeability index (PI) and magnesium hazard (MH) reveal that most of groundwater is relatively appropriate for Agricultural purposes. Our findings, which include information on aquifer geometry, groundwater potential, quality, and usability, are anticipated to be helpful in managing groundwater issues in the area and other locations with comparable geologic settings and issues.

References

Abdalla, F., 2012. Mapping of groundwater prospective zones using remote sensing and GIS techniques: a case study from the Central Eastern Desert, Egypt. J. Afr. Earth Sci.70, 8–17.

Abdalla, F., Moubark, K., & Abdelkareem, M. (2020). Groundwater potential mapping using GIS, linear weighted

combination techniques and geochemical processes identification, west of the Qena area, Upper Egypt. Journal of Taibah University for Science, 14(1), 1350-1362.

Abdel Moneim, A. A. (2005). Overview of the geomorphological and hydrogeological characteristics of the Eastern Desert of Egypt. Hydrogeology Journal, 13(2), 416-425.

Ageeb, G. W.,Kotb, M. M. ,Rahim, I. S., (2007). Soil mapping of Wadi Hodein Area, Southeastern Egypt using remote sensing and GIS techniques. Aust. J. Basic Appl. Sci.1(4),793–800.

Ahmed, A. A., Shabana, A. R., & Saleh, A. A. (2019). Using hydrochemical and isotopic data to determine sources of recharge and groundwater evolution in arid region from Eastern Desert, Egypt. Journal of African Earth Sciences, 151, 36-46.

Alemayehu, T., Leis, A., & Dietzel, M. (2020). Environmental isotope and hydrochemical characteristics of groundwater in central portion of Mekelle sedimentary outlier, northern Ethiopia. Journal of African Earth Sciences, 171, 103953.

Alezabawy, A.K., Basheer, A.A. & Selim, .S.I. (2021). Delineation and Evaluation of the Groundwater of Fractured Limestone Aquifer at East of Al Kurimat Area, Egypt: Geophysical and Hydrogeochemical Constraints. Pure Appl. Geophys. 178, 4425–4459 (2021). https://doi.org/10.1007/s00024-021-02840-w.

Alharbi TG, Zaidi FK (2018) Hydrochemical classification and multivariate statistical analysis of groundwater from Wadi Sahba Area in Central Saudi Arabia. Arab J Geosci 11:643.

Ali-Bik, M. W., Sadek, M. F., & Hassan, S. M. (2022). Basement rocks around the eastern sector of baranis-aswan road, Egypt: Remote sensing data analysis and petrology. The Egyptian Journal of Remote Sensing and Space Science, 25(1), 113-124.

Arafat, A. A., Salama, M. H. M., El-Sayed, S. A., & Elfeel, A. A. (2017). Distribution of natural radionuclides and assessment of the associated hazards in the environment of Marsa Alam-Shalateen area, Red Sea coast, Egypt. Journal of radiation research and applied sciences, 10(3), 219-232.

Araffa SAS (2010). Geophysical investigation for shallow subsurface geotechnical problems of Mokattam area, Cairo, Egypt, Environmental earth sciences journal, Vol. 59, 1195-2207.

Araffa SAS, El Shayeb HM, Abu Hashesh MF, Hassan NM (2015). Delineating subsurface structure and assessment of groundwater aquifer using integrated geophysical interpretation at the central part of Sinai. Arabian Journal of Geosciences. AJGS, Egypt, 8, No. 10, 7993-8007.

Araffa, S. A. S., Mohamed, A. M., & Santos, F. M. (2017). Geophysical investigation in the Northwestern part of the Gulf of Suez, Egypt. Egyptian journal of petroleum, 26(2), 457-475.

Ayers RS, Westcot DW (1985). Water quality for agriculture. FAO irrigation and drainage paper, 29, Rev. 1. P 192.

Azab, M. A. (2009, April). Flood hazard between Marsa Alam—Ras Banas, Red Sea, Egypt. In Fourth Environmental Conference, Faculty of Science, Zagazig University (pp. 17-35).

Babatunde A, Olubusola IS, Tope JE, Karram AA, Kolawole AA, & Taiwo AN (2022). Hydrogeophysical Investigation Using Electrical Resistivity Method within Lead City University Ibadan, Oyo State, Nigeria. International Journal of Earth Sciences Knowledge and Applications, 23 4(1), 51-62.

Basheer AA., Alezabawy AK (2020). Geophysical and hydrogeochemical investigations of Nubian sandstone aquifer, South East Sinai, Egypt: Evaluation of groundwater distribution and quality in arid region, Journal of African Earth Sciences, Volume 169, 103862, 2020, https://doi.org/10.1016/j.jafrearsci.2020.103862.

Brindha, K., Pavelic, P., Sotoukee, T., Douangsavanh, S., Elango, L., (2017). Geochemical characteristics and groundwater quality in the Vientiane Plain. Laos. Expo. Health 9 (2), 89–104.

Chouchene AB, Lachaal F, Zouhri L, Boualaares A & Gabtni H (2022). The uses of geophysical methods in hydrogeological study of Grombalia plain (Northeastern Tunisia). Arabian Journal of Geosciences, 15(1), 1-15.

Datta, P. S., & Tyagi, S. K. (1996). Geochemical processes controlling groundwater quality in Pushkar Valley, Rajasthan, India. In Quaternary Deserts and Climatic Change (pp. 397-401). CRC Press.

Detay, M. and M. Carpenter, (1997). Water wells: implementation, maintenance and restoration.Wiley, London.

Doneen LD (1964). Notes on water quality in agriculture. Published as a water science and engineering paper 4001, Department of Water Science and Engineering, University of California, Davis.

EGSMA (Egyptian Geological Survey and Mining Authority), (1997). Geologic map of Hamata Quadrangle Egypt, sheet No. NG 36 G, Scale 1: 250,000. Cairo, Egypt:EGSMA.

Embaby, A., & Ali, M. (2021). Hydrogeochemical processes controlling groundwater in Western Sohag Governorate, Upper Egypt. Arabian Journal of Geosciences, 14(9), 1-18.

Freeze RA, Cherry JA (1979). Groundwater (No. 629.1 F7). Prentice-Hall, Englewood Cliffs, NJ 07632f

Gaillardet, J., Dupre, B., Louvat, P., Allegre, C.J., (1999). Global silicate weathering and CO_2 consumption rates deduced from the chemistry of large rivers. Chem. Geol. 159,3–30.

Gheith, H., Sultan, M., (2002). Construction of a hydrologic model for estimating Wadi runoff and groundwater recharge in the Eastern Desert, Egypt. J. Hydrol. 263, 36–55.

Gibbs, R.J., (1970). Mechanisms controlling world water chemistry. Science 170,1088–1090 (80-.).

Hwang, J. Y., Park, S., Kim, M. S., Jo, H. J., Lee, G. M., Shin, I. K., & Kim, H. K. (2017). Applications of hydrochemical models for the assessment of groundwater. Environ Nat Resour Res, 20(3), 156-173.

Khalil,M.H., (2014). Detection of magnetically susceptible dykes warms in a fresh coastal aquifer. Pure Appl. Geoph.171,1829–1845. Springer Basel.

Kumar PJS (2016). Deciphering the groundwater–saline water interaction in a complex coastal aquifer in South India using statistical and hydrochemical mixing models. Model Earth Syst Environ 2:194. https://doi.org/10.1007/s40808-016-0251-2.

Kumar, M., Ramanathan, A.L., Ranjan, S., Singh, V.B., Kumar, N., Yadav, S.K., Rao, M.S., Ritch, S., Bhattacharya, P., (2018). Groundwater evolution and its utility in upper Ganges-Yamuna Alluvial plain of Northern India, India: Evidence from solute chemistry and stable isotopes. Groundw. Sustain. Dev. 7, 400–409.

Lankester, F. (2012). Predynastic & Pharaonic era Rock-Art in Egypt's Central Eastern Desert: Distribution, Dating & Interpretation (Doctoral dissertation, Durham University).

Matthes, G., (1982). The Properties of Groundwater. John Wiley and Sons, New York, 406.In: ISBN0–471–08513-8.

McLean, W., Jankowski, J., (2000). Groundwater quality and sustainability in an alluvial aquifer, Australia. In: Sililo, et al. (Ed.),

Proc. XXX IAH congress on Groundwater:Past Achievements and Future Challenges. Cape Town South Africa 26th November–1st December 2000. AA Balkema, Rotterdam, Brookfield.

Mohamaden, M. I., & Ehab, D. (2017). Application of electrical resistivity for groundwater exploration in Wadi Rahaba, Shalateen, Egypt. NRIAG Journal of Astronomy and Geophysics, 6(1), 201-209.

Mohamed A. M. E., Araffa S. A. S, Mahmoud N. I. (2012). Delineation of Near-Surface Structure in the Southern Part of 15th of May City, Cairo, Egypt Using Geological, Geophysical and Geotechnical Techniques. Pure and Applied Geophysics, 169, No. 9, 1641-1654.

Mosaad S, Basheer AA (2020). Utilizing the Geophysical and Hydrogeological Data for the Assessment of the Groundwater Occurrences in Gallaba Plain, Western Desert, Egypt. Pure Appl. Geophys. 177, 3361-3382 (2020). https://doi.org/10.1007/s00024-019-02414-x.

Mthembu, P. P., Elumalai, V., Brindha, K., & Li, P. (2020). Hydrogeochemical processes and trace metal contamination in groundwater: impact on human health in the Maputaland coastal aquifer, South Africa. Exposure and Health, 12(3).

Mukherjee, A., Fryar, A.E., Thomas, W.A., (2009). Geologic, geomorphic and hydrologic framework and evolution of the Bengal basin, India and Bangladesh. J. Asian Earth Sci. 34, 227–244.

Naseem, S., Rafique, T., Bashir, E., Bhanger, M.I., Laghari, A., Usmani, T.H., (2010). Lithological influences on occurrence of high-fluoride groundwater in Nagar Parkar area, Thar Desert, Pakistan. Chemosphere 78 (11), 1313–1321.

Nowroozi, A. A., Horrocks, S. B., & Henderson, P. (1999). Saltwater intrusion into the freshwater aquifer in the eastern shore of Virginia: a reconnaissance electrical resistivity survey. Journal of Applied Geophysics, 42(1), 1-22.

Paliwal, K.V., (1967). Effect of gypsum application on the quality of irrigation waters. Madras Agric. J. 59, 646–647.

Papazotos P, Koumantakis I, Vasileiou E (2019). Hydrogeochemical assessment and suitability of groundwater in a typical Mediterranean coastal area: A case study of the Marathon basin, NE Attica.Greece HydroResearch 2(2019):49–59.

Paul, R., Brindha, K., Gowrisankar, G., Tan, M.L., Singh, M.K., (2019). Identification of hydrogeochemical processes controlling groundwater quality in Tripura, Northeast India using evaluation indices, GIS and multivariate statistical methods. Environ. Earth Sci. 78 (15), 470.

Pillsbury AF, Blaney HF (1966). Salinity problems and management in river-systems. J Irrig Drain Div 92:77–90.

Piper AM (1994) A graphical procedure in the geochemical interpretation of water analysis. Am Geophys Union Trans 25:914–928.

Rajimohan N, Elango L (2004) Identification and evaluation of hydrogeochemical processes in the groundwater environment in an area of the Palar and Cheyyar river basins, southern India. Environ Geol 46:47–61

Res1D, V1 beta, (2001). Geometrical software, Interpretation Modeling for Vertical Electrical Sounding, https://www.geotomosoft.com/index.php, the Applied Geophysics Unit of University College Galway, Ireland.

Revelle, R. (1941). Criteria for recognition of the sea water in ground-waters. EOS. Transactions of the American Geophysical Union, 22, 593–597. https://doi.org/10.1029/TR022i003p00593.

Richards, L.A., (1954). Diagnosis and Improvement of Saline and Alkali Soils, Vol. 78.LWW, p. 154, 2.

Schoeller, H., (1965). Qualitative evaluation of groundwater resources. Methods Tech.Groundw. Investig. Dev. UNESCO 5483.

Stuyfzand, P. J. (1986, May). A new hydrochemical classification of water types: principles and application to the coastal dunes aquifer system of the Netherlands. In 9th Salt Water Intrusion Meeting, Delft (pp. 12-16).

Sultan SA, Santos FAM (2008). Evaluating subsurface structures and stratigraphic units using 2D electrical and magnetic data at the area north Greater Cairo, Egypt. International Journal of Applied Earth Observation and Geoinformation, 10, No. 1, 56-67.

Szabolcs, I., & Darab, C. (1964). The influence of irrigation water of high sodium carbonate content of soils.In Proceedings of 8th international congress of ISSS,Trans, II (pp. 803–812).

TDA/RSSTI (Tourism Development Authority and Red Sea Sustainable Tourisim Initiative). (2003). Land use management plan, south Marsa-Alam, Red Sea Coast, Egypt: USAID, Egypt, Report by PA Consulting Group prepared for Tourism Development Authority, Red Sea Sustainable Tourism Initiative, Contract/Order No. LAG- 1-00-99-00019-00. Task Order No. 807, 47p.

Todd, D. K. (1980). Groundwater hydrology, 2nd Edn.New York: Wiley.

US Salinity Laboratory Staff. (1954). Diagnosis and improvement of saline and alkali soils. USDAAgricultural Handbook No. 60. U.S. Government Printing Office, Washington, D.C.

WHO (2011). Guidelines for drinking-water quality, 4th edn. World Health Organization, Geneva.

Wilcox LV (1955). Classification and use of irrigation waters. USDA Circular 969. US Department of Agriculture, Washington, DC.

Wilcox, L.V. Classification and Use of Irrigation Waters; U.S. Dept. of Agriculture: Washington, DC, USA, 1995.

Yidana, S. M., Dzikunoo, E. A., Aliou, A. S., Adams, R. M., Chagbeleh, L. P., & Anani, C. (2020). The geological and hydrogeological framework of the Panabako, Kodjari, and Bimbilla formations of the Voltaian supergroup–Revelations from groundwater hydrochemical data. Applied Geochemistry, 115, 104533.

Yousef, A.F., Salem, A.A., Baraka, A.M., Aglan, O.S., (2009). The impact of geological setting on the groundwater occurrences in some wadis in Shalatein-abu Ramad area, south Eastern Desert, Egypt. Eur. Water Pub.(EWRA) 25, 53–68.

Zagloul, A., Elewa, H. H., & Abd El-Samie, S. G. (2000). Ground Water Evolution in Halaib and Shalatein Area, South-East Egypt as Indicated by Hydrochemistry and Environmental Isotopes. Isotope and Radiation Research, 32, 1-11.

Zaidi FK, Nazzal Y, Ahmed I, Al-Bassam AM, Al-Arifi NS, Ghrefat H, Al-Shaltoni SA (2015b) Hydrochemical processes governing groundwater quality of sedimentary aquifers in Central Saudi Arabia and its environmental implications. Environ Earth Sci 74:1555–1568.

ZondTEM1D (2016). one-dimensional multi-stations interpretation(resistivity, IP and magnetic permeability) of Transient ElectroMagnetic(TEM) and frequency sounding for various observation systems [Line/Loop, Loop/Loop, Loop/Line, Line/Line) ground and airborne, http://zond-geo.com/english/zond-software/electromagnetic-sounding/zondtem1d/.